BNL 39351
INFORMAL REPORT

OZONE PRODUCTION AT THE NATIONAL SYNCHROTRON LIGHT SOURCE

Christopher Weilandics[1]
Norman Rohrig[1]
Nicholas F. Gmur[2]

BNL--39351

DE87 007642

[1]Safety and Environmental Protection Division
Building 535A
and
[2]National Synchrotron Light Source
Building 510E

Brookhaven National Laboratory
Upton, NY 11973

January 1987

Research Supported by the
OFFICE OF BASIC ENERGY SCIENCES
U.S. DEPARTMENT OF ENERGY
WASHINGTON, D.C.

NATIONAL SYNCHROTRON LIGHT SOURCE
BROOKHAVEN NATIONAL LABORATORY
Associated Universities, Inc.

Under contract No. DE-AC02-76CH00016 with the
United States Department of Energy

DISCLAIMER

TABLE OF CONTENTS

ABSTRACT

Ozone production by synchrotron radiation as a function of power density in air was investigated using a white beam at the BNL National Synchrotron Light Source (NSLS) x-ray ring. Power densities were calculated from the energy spectrum at 2.52 GeV. Ozone concentrations in small beam pipes were measured for power densities between $I = 10^{12}$ and 10^{15} $eV \cdot cm^{-3} \cdot sec^{-1}$. The measured ozone half-life was 37 ± 2 min. The measured G-value was 2.69 ± 0.14 mol/100 eV and the ozone destruction factor k was less than 7×10^{-19} $cm^3 \cdot eV^{-1}$. The random uncertainties stated are approximately one standard error. The large departure of the values for G and k from previous values suggest that some undiscovered systematic error may exist in the experiment. Ozone concentration in excess of the 0.1 ppm ACGIH TLV can be generated in the experimental hutches but can readily be controlled. Industrial hygiene aspects of operation and possible control measures will be discussed.

INTRODUCTION

If one irradiates a given volume of air with photons ($E > 5.12$ eV), ozone will be formed by dissociation of the oxygen molecule and subsequent attachment of the atomic oxygen to another oxygen molecule (1). The rate of ozone concentration increase and the saturation point reached will be determined by: 1) the ozone formation rate, 2) the amount of energy deposited in a given volume, 3) the destructive action of the radiation on the ozone molecules, and 4) the chemical lifetime of ozone. When there is ventilation within the chamber, one must also consider 5) the air replacement rate for the chamber.

In this experiment a collimated beam of synchrotron radiation (SR) from a 2.52 GeV electron synchrotron irradiated the air in a series of chambers. The energy deposited in each chamber was calculated from the x-ray spectrum and the attenuation in air.

Ozone production from an electron beam has been measured (2,3), but no measurements have been reported from that induced by synchrotron radiation. This paper provides data on ozone production by a white beam and a technique for predicting ozone levels in an experimental hutch from the beam line configuration. Based on anticipated levels, specific remedial action may be taken.

HEALTH EFFECTS

Ozone is an irritant of the respiratory system, eyes, skin, and mucous membranes. Particularly susceptible to injury is the lower region of the lungs, especially the transitional region from the bronchioles to the alveoli (4). Chronic exposure to ozone can result in changes in lung morphology and function, and can contribute to tumor formation and aging (4). In sufficient quantities, ozone is capable of causing death in animals from pulmonary edema. Acute ozone effects in humans are listed in Table 1. Concentrations below which acute effects can be seen have been shown to cause increased susceptibility to airborn infections. For example, enhanced mortality in mice was observed following challenges by bacterial aerosols after exposure to ozone at 0.08 ppm for three hours (5).

The current eight hour Threshold Limit Value (TLV) is set by the American Conference of Governmental Industrial Hygienists (ACGIH) at 0.1 ppm (0.2 $mg \cdot m^{-3}$) with a Short Term Exposure Limit (STEL) of 0.3 ppm (6). Low concentrations of ozone (0.01 - 0.05 ppm) have a perceptible odor; the threshold for smell may be as low as 0.5 ppb to as high as 1.2 ppm (7).

Table 1. Acute Ozone Effects in Humans

O_3 (ppm)	Exposure Period	Effects
0.10+	1 hour	Increased airway resistance
0.30+	Cont. working hrs.	Nose and throat irritation, chest constriction
0.65*	6 - 10 hours	Minor chromosomal abnormalities
2.00+	2 hours	Severe cough

+NAPCA, 1970 (8)
*NAS, 1977 (9)

BASICS OF OZONE PRODUCTION

The mechanism for generation of ozone is dissociation of oxygen molecules by low energy (eV) photons and subsequent attachment to another oxygen molecule. As higher energy (keV) photons interact with matter, a number of low energy photons are generated. The total number of low energy photons and thus ozone molecules produced is proportional to the total energy absorbed from the spectrum of photons.

Assuming uniform mixing in a chamber, the generation and dissipation of ozone in it can be described with the following differential equation:

$$dC/dt = \left(\frac{GI}{100n}\right) - \alpha C - \beta C - kIC \qquad (1)$$

where:

C = concentration of ozone molecules (ppm)

G = value for ozone formation (# molecules/100 eV)

I = power density or mean energy deposited per unit time and volume ($eV \cdot cm^{-3} \cdot sec^{-1}$)

n = 2.462×10^{13} mol/cm^3 per ppm at 25° C

α = chemical decay constant for ozone (sec^{-1})

β = the ventilation rate divided by the chamber volume (sec^{-1})

k = a constant describing the destructive action of the beam on ozone ($cm^3 \cdot eV^{-1}$)

The solution of this equation is:

$$C(t) = \frac{GI}{100n(\alpha+\beta+kI)} [1-e^{-(\alpha+\beta+kI)t}] = C_{sat}(1-e^{-\lambda t}) \qquad (2)$$

where C(t) equals the ozone concentration after t seconds of irradiation; C_{sat} equals the ozone saturation concentration. After the beam is turned off, the concentration will decay according to:

$$C(t') = C_o \, e^{-(\alpha+\beta)t'} \qquad (3)$$

where C_0 equals the initial O_3 concentration and t' equals the time of ventilation after the beam has been turned off. If the exhaust or sampling system is turned off (β=0), only the chemical decay is operative.

For photons of a particular energy, energy absorbed is the product of the photon energy, the number of photons, and the fraction of photons absorbed. The total power absorbed, P, is simply the integral of this product over the photon energy spectrum. The fraction of photons absorbed is given by $(1-\exp(-\mu_a x))$ where μ_a is the energy absorption cross-section and x is the target thickness, the units being chosen to cancel out. The number of photons is that from the initial synchrotron radiation spectrum reduced in number by collimators and the attenuation in upstream absorbers. The attenuation is given by $(\exp(-\mu_t x))$ where μ_t is now the total cross-section.

SYNCHROTRON RADIATION SPECTRUM

Synchrotron radiation is produced when relativistic electrons are accelerated radially by a magnetic field. The spectrum of synchrotron radiation as derived by Schwinger (10) follows from classical electrodynamic theory as modified Bessel functions of fractional order. The continuous energy spectrum may be described by a critical energy (5.07 keV in this experiment) with one half of the power emitted above and below this energy. The vertical angular spread of the photon beam from the electron path is about 0.2 mrad for 2.52 GeV electrons and results from the Lorentz transformation of the radiation pattern from the electron rest frame to the laboratory frame.

The synchrotron spectrum was calculated using the iterative routine introduced by Kostroun (11) to calculate the Bessel function integrals. This routine is simple enough to implement on a programmable calculator. The initial calculations of spectrum and the energy deposited in the gas were calculated on a Hewlett-Packard calculator using the total vertical spectrum. Based on these calculations, the experimental chamber dimensions were chosen to provide power depositions differing by an order of magnitude between chambers. Use of the attaching adapters and the aluminum foils separating the chambers caused different ratios.

The energy depositions used in the data analysis were subsequently calculated with a FORTRAN program initially developed by Suortti and Thomlinson (12) to calculate beam heating effects and later modified by D. Chapman, N. Gmur and N. Lazarz (NSLS report in preparation). This program uses the Kostroun routine and calculates the vertical distribution and the integral of the photon fluence. Apertures and absorbers can be inserted sequentially to simulate an experimental arrangement. The two calculations agreed when the vertical apertures in the FORTRAN version were deleted. The power deposition values are given in Table 2 for a nominal 50 mA beam and 1 mrad of horizontal acceptance angle. The average power

densities I ($eV \cdot cm^{-3} \cdot sec^{-1}$) for each chamber were determined by dividing the power deposited P($eV \cdot sec^{-1}$) along the path length for each chamber by the chamber volume (cm^3). The in-beam power densities are much larger (by a factor of 50 to 1200) because only part of each chamber is irradiated.

Table 2. Chamber Parameters and Power Deposition Rates (50 mA, 1 mradh)

Chamber Section	Chamber Length (cm)	Chamber Volume (cm^3)	Sampling Rate ($cm^3 \cdot min^{-1}$)	β (sec^{-1})	Power Deposition ($eV \cdot sec^{-1}$)	Power Density ($eV \cdot cm^{-3} \cdot sec^{-1}$)
I+	35.4	662.0	494.5	1.295E-2	3.023E18	4.566E15
II@	161.3	11611.0	494.5	7.098E-4	1.930E18	1.662E14
III*	22.9	7135.0	1000.0	2.336E-3	1.200E17	1.682E13

+downstream of a 0.25 mm Beryllium window
@also downstream of a 0.025 mm Aluminum window
*downstream of a second 0.025 mm Aluminum window

Figure 1 shows the photon spectra entering the second chamber after the aluminum window and following the 1.6 m air path. The energy deposited in the second chamber is the difference between the curves and is primarily due to 6 to 15 keV photons. The unfiltered fluence at low energies approximately follows an exponential increase with decreasing energy. Each filter material essentially cuts off the photons below particular energies which are largely influenced by the photoelectric cross-section and thus the Z of the material. The important energies in the first chamber following the beryllium window are between 2 and 10 keV, while those between 8 and 15 keV are important in the third chamber.

MATERIALS AND METHODS

Description of the X13A Beam Line

As explained above, ozone is formed if synchrotron radiation greater than 5.12 eV is passed through the atmosphere. In order to study this generation of ozone, a white beam line and hutch were required. These were provided on beam line X13A by Dr. David Cox. A description of the beam line characteristics is given in Fig. 2 (13). A diagram of the beam line layout is given in Fig. 3 (14). The experimental chambers for monitoring ozone generation were mated downstream of the beryllium window assembly via a KF flange.

Experimental Chambers for Monitoring Ozone Generation

Figure 4 shows the experimental apparatus in which ozone is generated when a white SR beam passes through the air-filled chambers. The stainless steel apparatus consists of three pipe sections (chambers), adaptors (Conflat flanges), and sampling tubes. As discussed previously, lengths and inner diameters were chosen so different power densities and thus ozone levels would be generated.

The atmosphere contained within each pipe section is isolated from the ambient and other pipe sections by 0.025 mm thick aluminum foil windows sandwiched in place between copper gaskets. In the first pipe section, the atmosphere is isolated from the upstream beam pipe ultra-high vacuum by a 0.25 mm thick beryllium window. Tubes (6.35 mm O.D.) placed at the ends of each pipe section allowed for air intake and outflow during sampling and analysis of ozone.

Beam Definition

The white synchrotron beam was defined vertically by a 2 mm slit opening which was not changed during the entire run. The horizontal acceptance angle was changed using computer addressed servos. The acceptance angle was measured for different slit settings by exposing a sheet of photographic paper at a known distance from the synchrotron beam source and measuring the burn dimensions.

The electron beam current in the storage ring was measured with a current transformer calibrated to within 1 percent of the true value. The electron beam energy was defined by the magnetic dipole field strength which was measured to within 2 percent of the true value.

Sampling Methods

Each chamber was sampled in one of two ways. In one scheme (see top of Fig. 5) the ozone meter pump was attached to one of the sampling tubes and pumped directly on the chamber. Make-up air was drawn into the chamber by negative pressure through the second sampling tube and the ozone concentration was read directly from the meter. In cases where the maximum concentration would exceed the maximum range of the instrument (10 ppm), air was pumped into the chamber (see bottom of Fig. 5) and a mixing tee was added on to the exit sample tube. Dilution air was mixed with the stream, extending the range of the instrument to 110 ppm.

All sampling line materials were selected to minimize reaction with (or decomposition of) ozone. The chambers and sampling nozzles were clean stainless steel, mixing tees were of glass, and a small section of Teflon tubing connected the chambers to the ozone monitors.

The sampling and dilution pumps (DuPont Model P4000 Constant Flow Air Sampling Pumps) would maintain a constant flow (± 5% of a set point) over the operating range (ΔP 25" H_2O up to 2000 $cm^3 \cdot min.^{-1}$; 1-10" H_2O at 4000 $cm^3 \cdot min.^{-1}$) and were calibrated using a bubble meter.

The portable ozone analyzer (Analytical Instrument Development Model 560) uses the EPA approved method of measuring the light from the vapor phase of the chemiluminescent reaction of ozone and ethylene and is capable of measuring ozone concentrations down to 1 part per billion.

OZONE DECAY MEASUREMENT

To determine α, the decay constant (sec^{-1}) corresponding to the chemical half-life of ozone, the SR beam was allowed to enter the chambers and produce ozone. The beam was then turned off, the chambers were removed from the beam line, and the ozone was allowed to decay. At six times

spread over several hours the large second chamber was sampled for a few seconds after moving the chamber to mix the gas. The slope of a least squares line fitted to all six data points shown in Fig. 6 yields a decay constant of (3.10 ± 0.15)E-4 sec^{-1} which corresponds to a half-life of 37 ± 2 minutes. This value was used in the calculations and is in good agreement with a figure of 35 minutes obtained by George (15). A significantly better fit can be obtained by fitting only the first five data points (for a decay constant of (2.72 ± 0.08)E-4 sec^{-1} or a half-life of 42.5 ± 1.2 minutes) but we have no basis for excluding the last point.

DATA TAKING, ANALYSIS, AND RESULTS

The measurements to determine G and k involved measuring the concentration as a function of time after the safety shutter in the beam line was opened. The concentration generally followed the exponential buildup of Eq. 2 with approximately the expected time dependence (see Fig. 7), but saturation had not always been reached. The concentration at saturation and the exponent were estimated by iterative fitting of the concentration data. The parameters I and β had been calculated, and the measurement of α was described in the previous section. The parameter k was extracted from the exponent ($\alpha+\beta+kI$) and the parameter G was determined from the saturation value. The values of k showed large variations from 5×10^{-18} to 4×10^{-16} $cm^3 \cdot eV^{-1}$. Variations in G also resulted for the different measurements so this analysis technique was discarded.

The time dependence of ozone concentration would be given by Eq. 2 if the system was well mixed at all times. The above technique probably failed because the concentration in the chamber is not uniform so the time dependence does not follow Eq. 2. The radiation is more intense at the front end of the chambers and only a small portion of the air near the center is irradiated. The only mixing is provided by convection and pumping to the sample.

The second technique used only the saturation concentration which was determined by fitting the data for the latter part of the runs. After determining saturation concentrations for each of the five runs, using a spread sheet program, the data were iteratively fitted to the form of Eq. 2 with G and k as unknowns. The best fit results in Table 3 have G = 2.69 ± 0.14 mol/100eV. The destruction parameter used was k = 0 and values up to k = 7 x 10^{-19} $cm^3 \cdot eV^{-1}$ fit the data. The best fit occurred with a nonphysical negative value for k of -8 x 10^{-19} $cm^3 \cdot eV^{-1}$.

This value of k is much smaller than the 1.4 x 10^{-16} $cm^3 \cdot eV^{-1}$ mentioned by Fasso et al. (16) and the value of G is also smaller than the 6 to 13.8 mol/100eV generally reported (3,17,18). The measured concentrations are much larger than can be calculated with the suggested value of k.

The difference in G may be an artifact resulting from beam heating. During our experiments we made no attempts to measure the temperature of the gas in the chambers or of the chambers themselves. Power absorption in the front chamber is about 0.1 W which will heat the sampling volume of air by about 15° K if no heat is lost. However, this estimated temperature increase is an average value with the in-beam value being much higher, probably causing convection within the chamber and complicating an estimate of local density. With the in-beam gas density lower than was assumed, the calculated power absorbed is high, so G is low.

Table 3. Measured and Calculated Saturation Concentrations

Ch.*	Ring Current (mA)	Horiz. Accept. (mrad)	Power Density ($eV \cdot cm^{-3} sec^{-1}$)	Calc. Conc. (ppm)	Meas. Conc. (ppm)	M-C** (ppm)	Conc. With No Venting (ppm)
III	52.3	0.143	2.52E12	1.04	0.96	-0.08	8.9
III	55.0	0.305	5.64E12	2.33	2.20	-0.06	20
II	55.0	0.305	5.58E13	59.72	57.10	-0.04	196
I	53.0	0.143	6.92E14	59.62	62.00	-0.04	2400
I	40.5	0.305	1.13E15	97.18	108.00	-0.11	4000

*Chamber section.
**Measured concentration minus calculated concentration.

IMPLICATIONS FOR THE NSLS

Eq. 2 may be used to estimate the ozone concentration in an experimental hutch. The ventilation rate β is pumping speed Q divided by the hutch volume V. The power density I is the power deposition P divided by the volume. We can rewrite Eq.2 as:

$$C_{sat}\ (ppm) = GP/100nV(\alpha+Q/V) = GP/100n(\alpha V+Q) \qquad (4)$$

This saturation activity is the average value over the hutch volume, with much higher values near the beam path and lower values in normally occupied spaces. The experimenter needs to know the power deposited in air, the hutch volume, and the fan capacity to determine the saturation value.

Beam lines at NSLS operating in the white beam mode typically have the beam exiting through a 0.25 mm Be window followed by a 0.025 mm Al window with vacuum between the windows to minimize formation of toxic products which may form on Be windows (19). Using these as initial "filters" in the algorithm described above, power deposition along path lengths of 2, 10, 30, 100, and 300 cm of air were calculated. Although the results of these calculations do not fit a strict power function, the power deposited, P in eV/sec, can be estimated to within 20% by the following equation:

$$P = 1.3 \times 10^{15}\ (D^{0.76})i\theta \qquad (5)$$

where D is the distance traveled in air by the white beam (cm),
i is the stored electron beam current (milliamps), and
θ is the horizontal acceptance angle of the beam line (milliradians).

This equation and the constants can be inserted into Eq. 4 yielding the following numerical formula:

$$C_{sat}(ppm) = 1.5\ [i(mA)\cdot\theta(mrad_h)\cdot D(cm)^{0.76}/(300V(m^3) + 1000Q(1/sec))] \qquad (6)$$

Consider a small hutch (V = 2mx3mx3m) with a ventilation rate of Q = 100 $l \cdot sec^{-1}$ (~200 cfm) and a 2 m air path (D). Assume the beam current i is 300 mA and the acceptance angle θ is 2 mradh. The saturated concentration is then 0.48 ppm, about five times the 8 hour TLV and 1.5 times the 15 min STEL. This example demonstrates very poor experimental design which could be eliminated by greatly shortening the path length of the beam through air.

In the design phase of the experiment it is best to minimize the length of the open beam path, this being an operating requirement at the NSLS. In the example above, ventilation of the hutch is a very effective means of reducing the concentration. Localizing the ventilation can be especially effective, possibly using an elongated hood or shroud placed just above the beam path, to capture the high ozone concentration, and coupled to a flexible duct to allow easy access to the experimental setup. Additionally, if the experiment permits, the void space between the beryllium and aluminum windows can be filled with a relatively high Z inert gas such as neon, argon, or krypton which will reduce the flux of low energy photons which contribute most strongly to ozone formation, particularly in short air paths (if a gas filter is used, Eq. 4 must be replaced with the result of a calculation using the actual conditions).

If high ozone concentrations are anticipated and no control measures can be implemented before experiments are to begin, the hutch may be allowed to ventilate after the beam has been turned off to reduce the ozone concentration in the hutch. The ventilation time t_V (sec), needed for waiting before a given concentration is reached is given by the following expression:

$$t_V = \ln (C/C_S)/(\alpha+Q/V) \qquad (7)$$

where C_S = the ozone concentration required for safe entry
(0.3 ppm = 15 minute maximum exposure);
C = the existing ozone concentration.

For our hypothetical trial with a saturation concentration of 0.48 ppm, the time needed until the ozone concentration drops to 0.3 ppm (only a few minutes access being required) is about 80 seconds.

CONCLUSIONS

Measurements of ozone concentration were analyzed to determine the ozone production efficiency of synchrotron radiation, the chemical half-life, and a coefficient describing destruction of ozone by synchrotron radiation. The best fit half-life is 37 ± 2 minutes which is consistent with other measurements. The ozone production efficiency was G = 2.69 ± 0.14 mol/100eV which is lower than many values reported in the literature. Our measurements indicate that synchrotron radiation does not destroy ozone ($k < 7 \times 10^{-19}$ $cm^3 \cdot eV^{-1}$) in contrast to other reported results at much lower power densities where $k = 1.4 \times 10^{-16}$ $cm^3 \cdot eV^{-1}$.

We easily generated ozone levels at a thousand times the TLV. However, we have considered ozone control in experimental hutches and conclude that effective control is quite feasible. Suggested practices are: use short paths for the beam in air, ventilate the hutch near the ozone generation region, and filter the beam with an inert gas (N_2, Ne, Ar, or Kr) between the beryllium and aluminum windows.

ACKNOWLEDGEMENTS

The authors wish to thank the following individuals for their valuable assistance during this experiment: David Cox (Dept. of Physics) for the use of his X13A beam line; Peter Daum (DAS) and Daniel Leahy (DAS) for the loan of their ozone monitors and recorders; Stephen Schwartz (DAS) for his insights into the dynamics of ozone formation; and Richard Greene (NSLS) for the assembly of the ozone sampling chambers.

REFERENCES

1. Advances in Environmental Science and Technology 4, edited by J. N. Pitts, Jr., R. L. Metcalf, and A. C. Lloyd, John Wiley and Sons, NY, 1974.

2. P. Cavallucci, A. Esposito, M. Peliccioni, and A. Rindi, "Production of Ozone in Air by High Energy Electron Beams," Annali di Radio-protezione 1, 13, 1979.

3. C. Willis, A. W. Boyd, and M. J. Young, "Radiolysis of Air and Nitrogen-Oxygen Mixtures with Intense Electron Pulses: Determination of a Mechanism by Comparison of Measured and Computed Yields," Can. J. of Chem. 48, 1515-1525, 1970.

4. M. O. Amdur, "Air Pollutants," in Casarett and Doull's Toxicology, Second Edition edited by J. Doull, C. D. Klassen, and M. O. Amdur, 608-629, Macmillan Publishing Co., Inc., New York, 1980.

5. D. L. Coffin and E. J. Blommer, "Acute Toxicity of Irradiated Auto Exhaust, Its Indication of Enhancement of Mortality from Streptococcal Pneumonia," Arch. Environ. Health 15, 36-38, 1967.

6. Threshold Limit Values for Chemical Substances in the Workplace Environment Adopted by ACGIH with Intended Changes for 1985-1986, American Conference of Governmental Industrial Hygienists, 1985.

7. J. N. Ruth, "Odor Thresholds and Levels of Several Chemicals, A Review," Am. Ind. Hyg. Assoc. Journal 47, 142-151, 1986.

8. National Air Pollution Control Administration, "Air Quality Criteria for Photochemical Oxidants," ALP-63 HEW, Washington, DC, 1970.

9. National Academy of Sciences, "Ozone and Other Photochemical Oxidants," National Academy of Sciences, Washington, DC, 1977.

10. J. Schwinger, "On the Classical Radiation of Accelerated Electrons," Phys. Rev. 75, No. 12, 1912-1925, 1949.

11. V. O. Kostroun, "Simple Numerical Evaluation of Modified Bessel Functions $K_\nu(\chi)$ of Fractional Order and the Integral $\int_\chi^\infty K_\nu(\eta)d\eta$," Nuclear Instruments and Methods 172, 371-374, 1980.

12. P. Suortti and W. Thomlinson, "X-ray Filters for Synchrotron Radiation," National Synchrotron Light Source, Brookhaven National Laboratory, BNL No. 34934, 1984.

13. N.F. Gmur and S. White-DePace, "National Synchrotron Light Source Users Manual: Guide to the VUV and X-Ray Beam Lines", Brookhaven National Laboratory, 1986.

14. C. Foerster, R. Klaffky, N. Lazarz and W. Thomlinson, "National Synchrotron Light Source Beam Line Vacuum Procedures", Brookhaven National Laboratory, 1986.

15. A. C. George, A. J. Breslin, J. W. Haskings, Jr., R. M. Ryan, "Evaluation of the Hazard from Radioactive Gas and Ozone at Linear Accelerators," in Proc. USAEC First Symposium Accelerator Radiation Dosimetry and Experience, Brookhaven National Laboratory, CONF-651109, USAEC, Washington, DC., 513-555, 1965.

16. A. Fasso, K. Goebel, M. Hofert, G. Rau, H. Schonbacher, G. R. Sullivan, W. P. Swanson, and J. W. N. Tuyn, "Radiation Problems in the Design of the Large Electron-Positron Collider (LEP)," CERN 84-02, 20-21, 1984.

17. A. Brynjolfssun and T. G. Martin III., "Bremsstrahlung Production and Shielding of Static and Linear Accelerators Below 50 MeV," Int. J. Appl. Radiation Inst. 22, 36-37, 1971.

18. J.A. Ghormley, C.J. Hochanadel, and J.W. Boyle, "Yield of Ozone in the Pulse Radiolysis of Gaseous Oxygen at Very High Dose Rate. Use of This System as a Dosimeter," J. of Chem. Phys. 50(1), 419-423, 1969.

19. N.F. Gmur, "Analysis of Surface Contaminants on Beryllium Windows," National Synchrotron Light Source, Brookhaven National Laboratory, BNL No. 39091, 1986.

FIGURES

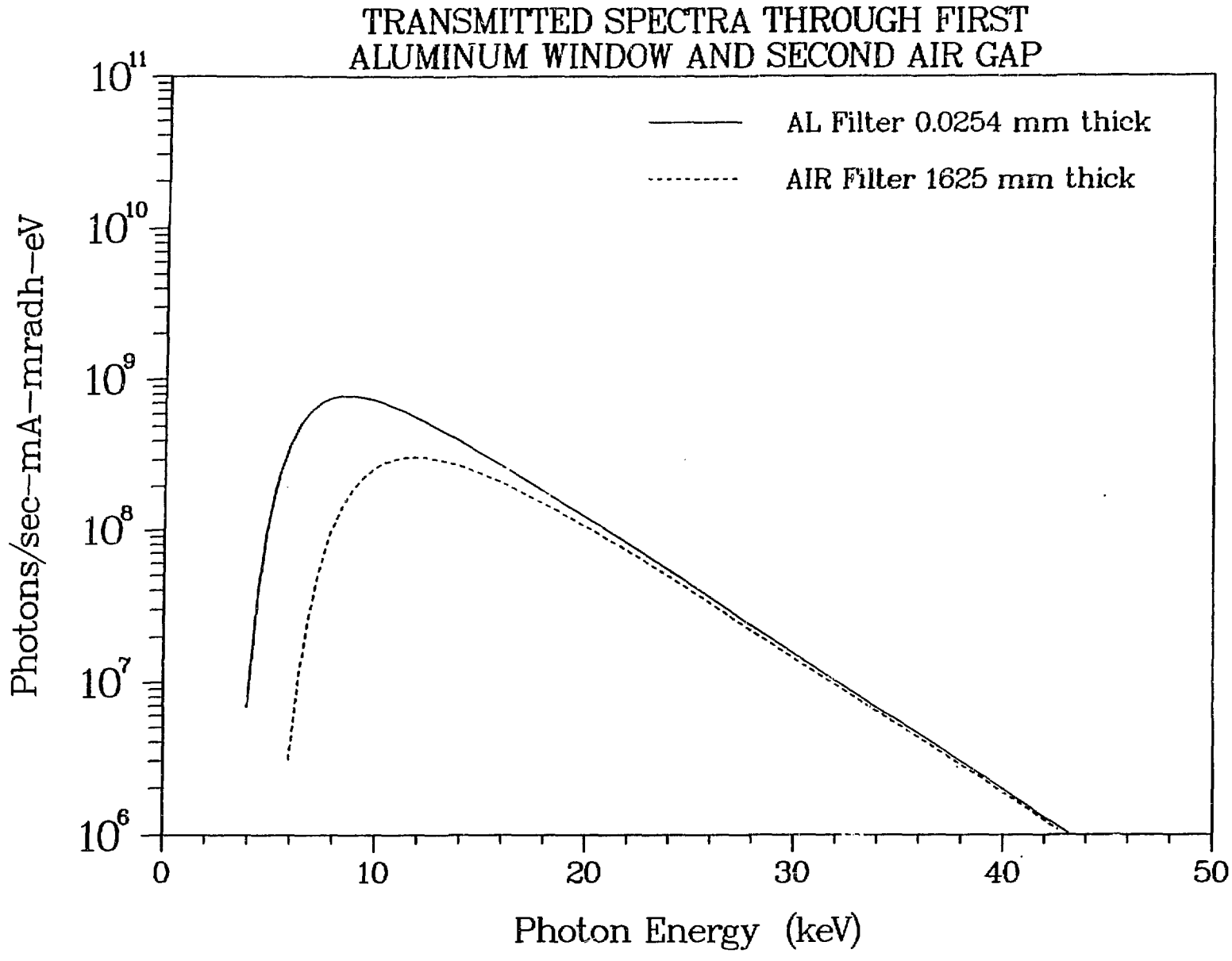

Figure 1. Synchrotron radiation spectra entering and exiting the second sampling chamber.

Beam Line:	**X13A**
Ring:	**X-Ray**
Operational Status:	**Operational**

Participating Institutions: National Synchrotron Light Source, Brookhaven National Laboratory - Physics Dept., University of Pennsylvania, State University of New York at Stony Brook and Alfred University, Allied Chemical, Dupont, Carnegie Institution of Washington, Union Carbide

Local Contact: David Cox (516) 282-5613, Brookhaven National Laboratory

Spokesperson: David Cox (516) 282-3818

Research Program: Powder diffraction

Energy Range (keV)	Crystal Type	Resolution ($\Delta E/E$)	Flux at sample (photons/sec)	Beam Size unfocused (mm)	Total Horizontal Angular Acceptance (mradians)
5-45	White Beam	Semiconductor detector $1 \div 2 \times 10^{-2}$ } Crystal analyzer $10^{-3} \div 10^{-2}$	5×10^{13}/keV @ 10 keV 4×10^{12}/keV @ 20 keV 5×10^{11}/keV @ 30 keV 7×10^{10}/keV @ 40 keV (100 mA, 2.5 GeV)	5.0 H x 2.5 V	2
5-20	Ge(111,220)	$2\times10^{-4} \div 10^{-3}$	2×10^{10} @ 8 keV (100 mA, 2.5 GeV)	5.0 H x 2.5 V	2

Optical Configuration:

a. White Beam Mode
Sample located 16 meters from source; beam size defined by remote-controlled variable slits with resolution of 2.5 μm yielding beam dimensions up to 20 mm horizontal and 2.5 mm vertical.

b. Monochromator Mode
Single flat crystal monochromator scattering in horizontal plane; sample scattering in vertical plane; located in hutch 16 meters from source (double crystal scattering in vertical plane available Fall 1986).

Experimental Apparatus

Radiation hutch; two-circle Huber θ-2θ goniometer system with vertical axis with x,y,z translations and two horizontal arcs; 2θ goniometer carries a horizontal arm on which is mounted a four-circle Huber diffractometer scattering in the vertical plane with an analyzer table and detector arm; various analyzer crystals available e.g. Ge(111), Ge(220), Ge(400), InSb(111), Si(111), graphite (004), LiF(200), quartz (101); ionization chamber; scintillation detectors; Si(Li) semiconductor detector; DISPLEX cryostat (20°-300°K) available summer 1986; Canberra Series 85 MCA (8K channels); furnaces available by the end of 1986.

Computer System Hardware and Software

LSI 11/23 computer to be upgraded to 11/73 by summer 1986; 80 MB Winchester; RX02 disk storage; 9-track magnetic tape drive; RSX11M operating system; CAMAC interface; Visual Effects 550 graphics terminal; LA50 printer; library of powder diffraction analysis programs available.

January 27, 1986

Figure 2. Description of X13A x-ray beam line.

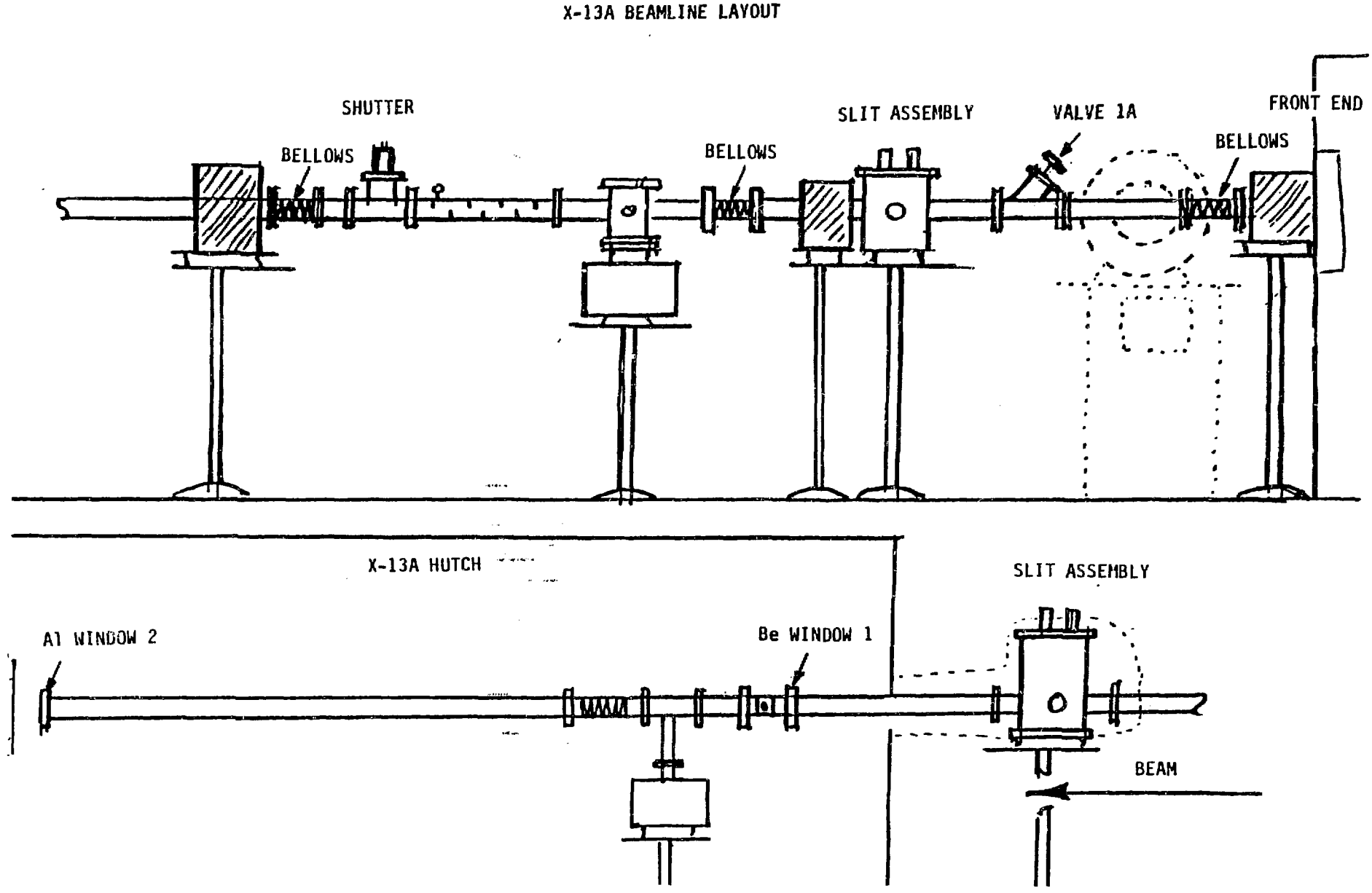

Figure 3. Layout of X13A x-ray beam line.

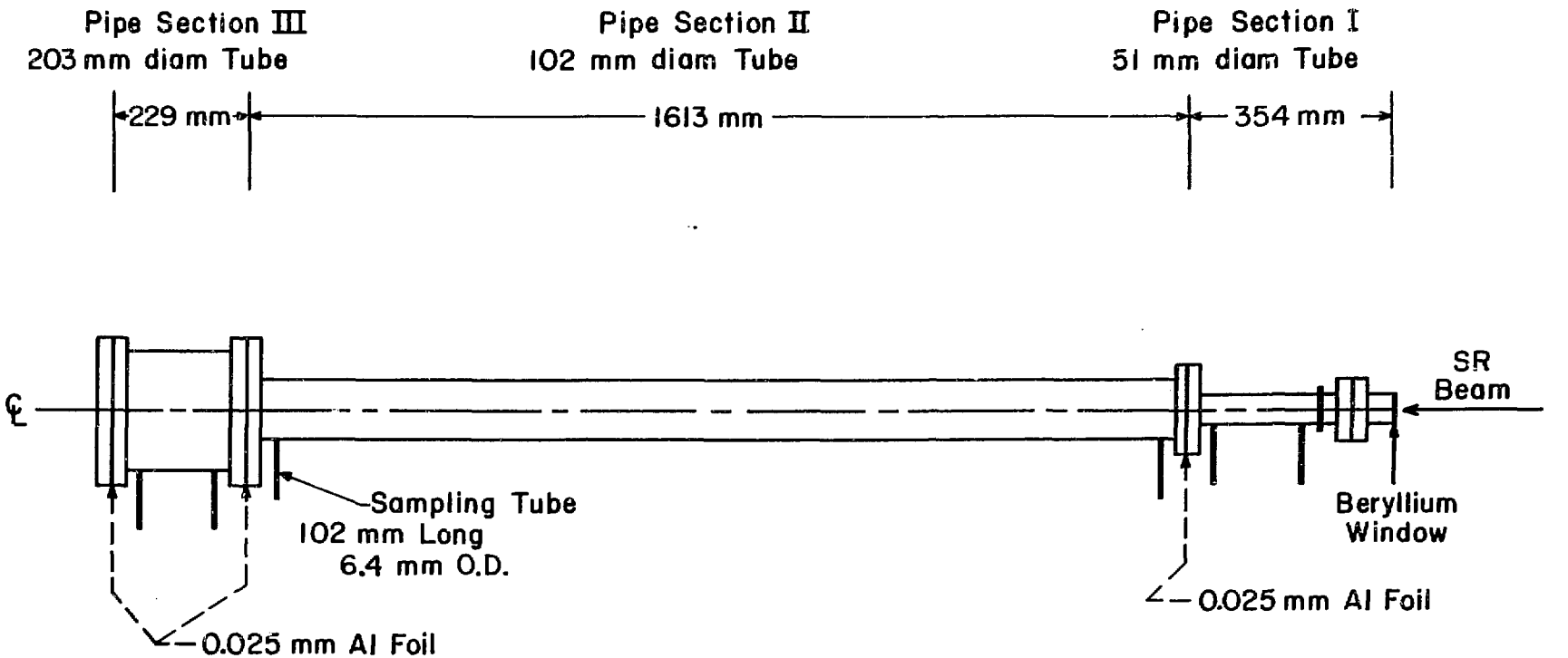

Figure 4. Ozone sampling chambers.

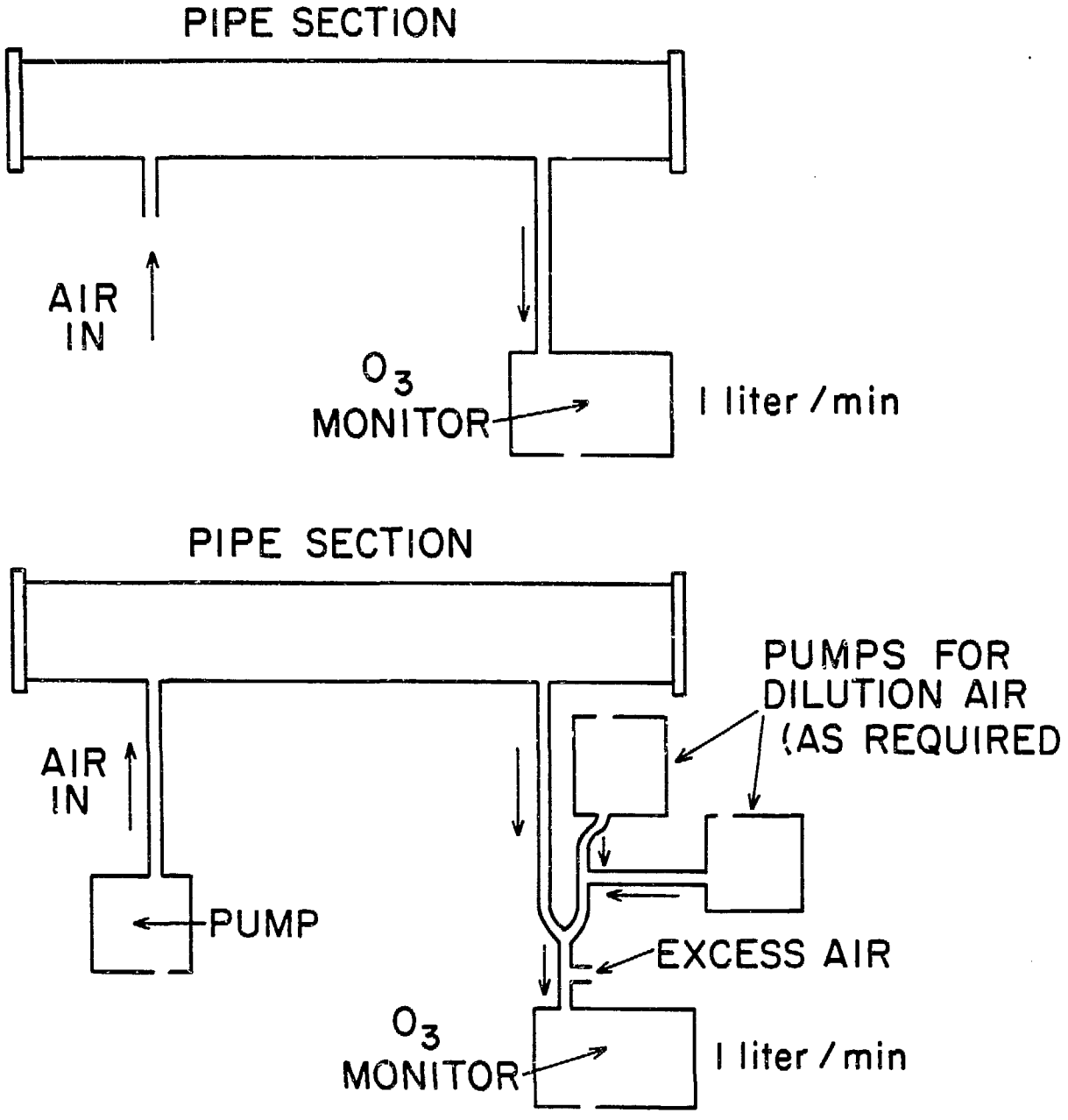

Figure 5. Ozone sampling arrangements.

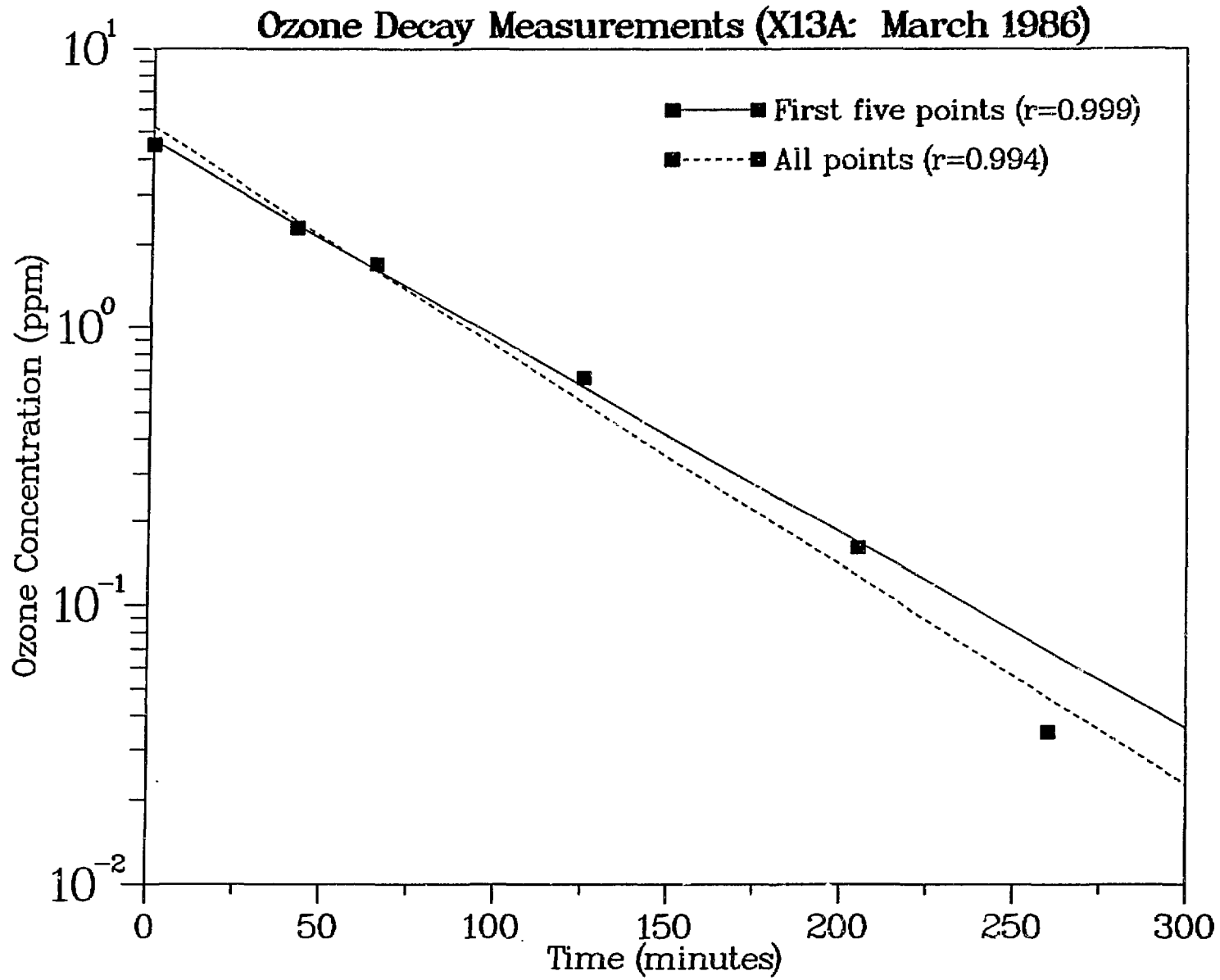

Figure 6. Ozone chemical decay measurement.

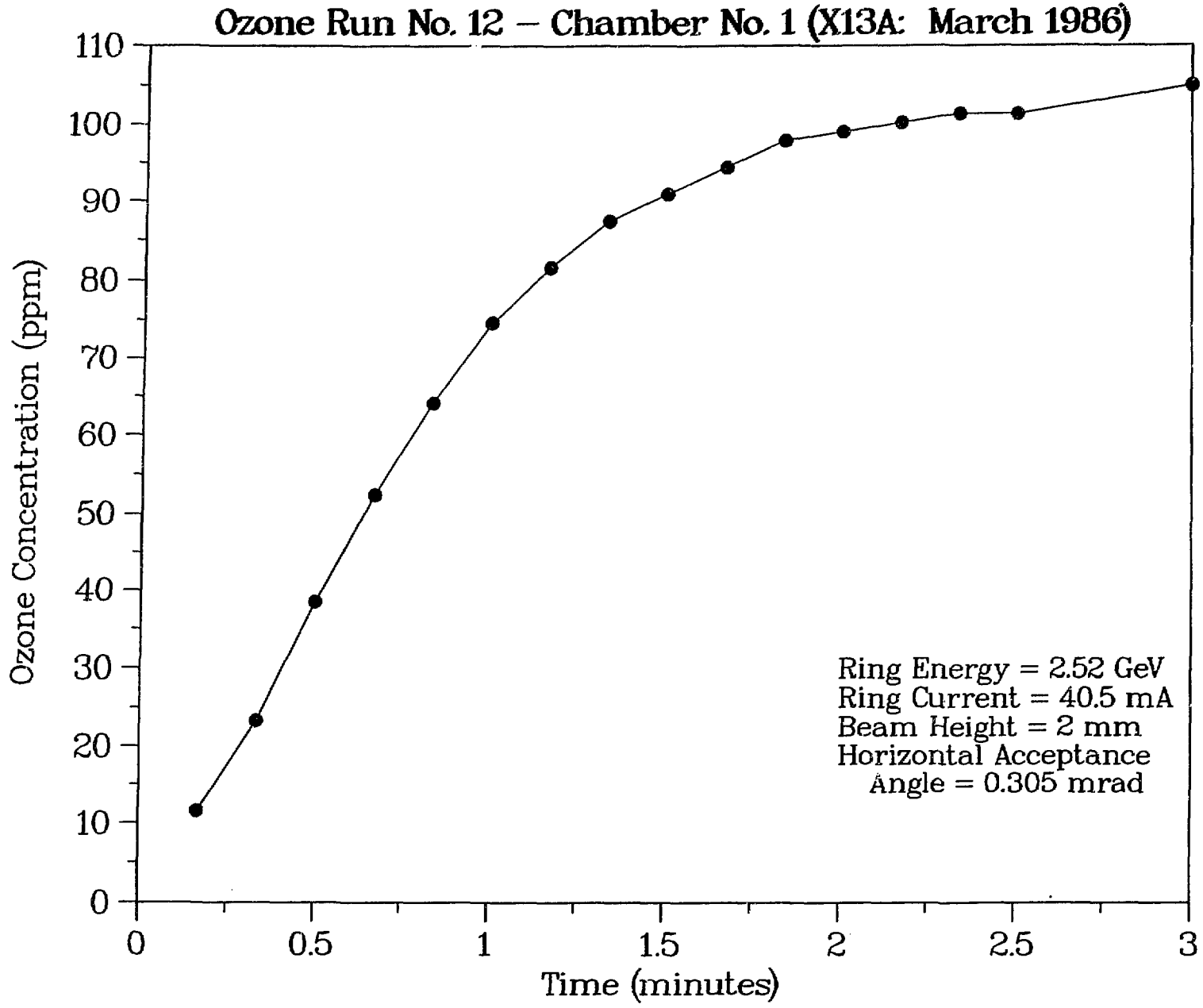

Figure 7. Ozone build-up and saturation in first sampling chamber.